Progress In Electromagnetics Research B, Vol. 49, 177–195, 2013

FORMULATION OF MULTIWIRE MAGNETIC TRANSMISSION-LINE THEORY

Jose A. Brandão Faria*

Instituto de Telecomunicações, Instituto Superior Técnico, Technical University of Lisbon, Av. Rovisco Pais, Lisboa 1049-001, Portugal

Abstract—Time- and frequency-domain theory of multiwire magnetic transmission lines is presented for the first time. The familiar theory of electric multiconductor transmission lines (MTL) is based on the manipulation of two matrices, the longitudinal impedance and the transverse admittance. However, for magnetic MTLs, the key matrices are the transverse impedance and the longitudinal admittance. It is shown how the latter matrices are defined and how they should be used to determine the modal propagation constants and modal characteristic wave admittances that characterize the various travelling wave modes of magnetic MTLs. The theory is illustrated considering a three-wire system with three-fold symmetry. Simulation results, in the range 0.1 GHz to 10 GHz, are presented, showing that the magnetic MTL can exhibit superluminal phase velocity and zero attenuation dispersion.

1. INTRODUCTION

Electric multiconductor transmission lines has been an important research topic for many decades; pioneering work on the matrix theory of MTL structures can be traced back to the late 1930s [1, 2]. With the advent of powerful computing tools, the topic kept attracting a wealth of attention until today [3–13]. The panorama is completely different as far as multiwire magnetic transmission lines are concerned.

The concept of a magnetic transmission line (MGTL) can be explained in quite simple terms. An MGTL is just the dual counterpart of an electric transmission line (ELTL). While an ELTL can be seen as an electric structure whose longitudinal conductors carry a time-varying current and where a transverse electric voltage exists between

Received 28 December 2012, Accepted 16 February 2013, Scheduled 19 February 2013

* Corresponding author: Jose Antonio Marinho Brandão Faria (brandao.faria@ist.utl.pt).

conductors, an MGTL can be seen as a magnetic structure whose longitudinal wires carry a time-varying magnetic flux and where a transverse magnetic voltage exists between wires. The theory, the fabrication, the technology, and the applications of MGTLs are, at this stage, a novel, open area of investigation. If a literature search on MGTLs is carried out, very scarce information will be found. In addition to [14–16], references to MGTLs can only be found in patent [17] dated of 1968 aimed at transients suppression in a power transformer, and also in a recent patent [18] where future terahertz applications of MGTL are speculated. The theoretical background for two-wire homogeneous magnetic transmission-line analysis has been set in [14], considering the quasi TEM approach. An application of MGTL theory to the analysis of ideal transformers has been provided in [15]. The evaluation of the per unit length magnetic reluctance of magnetic wires has been presented in [16] for the case of cylindrical Euler-Cauchy wires.

The contribution of the present paper to advancing the state of the art on MGTL is the extension of the two-wire formalism in [14] to the most general case of multiwire inhomogeneous systems. The multiwire MTL theory is illustrated through numerical simulations concerning a three-wire system with three-fold symmetry, where two degenerate modes (odd and even modes) can be defined. The application example takes into consideration the frequency-dependent character of the complex magnetic permeability of the wires. A comparison is established between the modal wave propagation parameters of the multiwire MGTL and its dual counterpart of a multiconductor ELTL with the same geometry.

2. FORMULATION OF MGTL PROPAGATION EQUATIONS

A cross-sectional view of the multiwire MGTL structure is presented in Figure 1. The $N+1$ wires, running parallel to the z axis, are made of a high-permeability material characterized by permeability μ_m. The wires are immersed in an inhomogeneous nonmagnetic linear dielectric medium, characterized by $\varepsilon = \varepsilon(x, y)$ and $\mu = \mu_0$. The magnetic fluxes ϕ_k in the multiwire system are assumed sufficiently weak to preclude nonlinearity phenomena.

As mentioned in [14], it must be emphasized that in the x, y transverse plane, the magnetic field is a purely gradient field $\nabla \times \mathbf{H} = 0$ (with open field lines, beginning and ending on different wires), and that the electric displacement vector is a purely solenoidal field $\nabla \cdot \mathbf{D} = 0$ (with closed field lines, embracing one or several wires). In

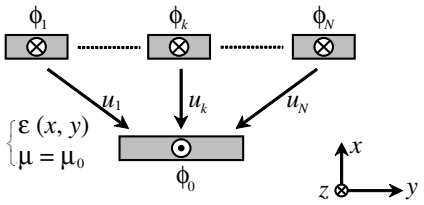

Figure 1. MGTL system with $N + 1$ wires. Magnetic voltages u_k and magnetic fluxes ϕ_k are indicated.

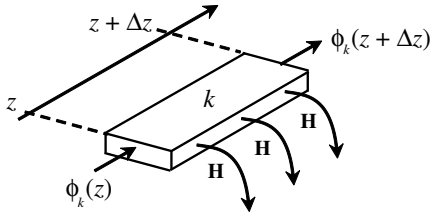

Figure 2. Field lines of **H** contribute to the transverse stray flux leaving the kth wire.

what follows the wire labeled 0 is taken as the reference magnetic wire (where the scalar magnetic potential is arbitrarily set to zero).

Time- and frequency-domain matrix equations, regarding the z-dependence of the magnetic voltages and magnetic fluxes along a magnetic MTL are determined in the next sections.

2.1. Time-domain Magnetic Flux Equation

Consider an infinitesimal segment of an MGTL of length Δz (see Figure 2). The closed surface containing the kth wire is traversed on the right by $\phi_k(t, z + \Delta z)$, is traversed on the left by $\phi_k(t, z)$, and its lateral surface is traversed by stray field lines of transverse magnetic field whose vector tips end on the remaining wires. The transverse magnetic field in the dielectric medium is the sum of transverse magnetic field individual contributions due to each magnetic wire, $\mathbf{H} = \sum_i \mathbf{H}_i$. The application of $\nabla \cdot \mathbf{B} = 0$ to Figure 2 yields the result in (1) where, due to linearity, the stray flux ϕ_k^{stray} can be written as a linear combination (superposition) of all the magnetic voltages $u_1 \ldots u_N$, yielding the result in (2), where g_{ki} are dimensionless real coefficients that only depend on the geometry of the MTL, and where each magnetic voltage [14, 19] is defined in (3), the open integration path $\overrightarrow{i0}$ belonging to the transverse plane. Note that in a transverse plane, where **H** is a gradient field, the concept of magnetic voltage is equivalent to magnetic scalar potential difference.

$$\phi_k(t, z + \Delta z) - \phi_k(t, z) = -\phi_k^{\text{stray}} \tag{1}$$

$$\phi_k^{\text{stray}} = \mu_0 \Delta z \sum_i g_{ki} u_i(t, z) \tag{2}$$

$$u_i(t,z) = \int_{\overrightarrow{i0}} \mathbf{H}_i(t,z) \cdot d\mathbf{s} \quad (\text{for } i = 1 \text{ to } N) \tag{3}$$

Substituting (2) into (1), making $\Delta z \to 0$, leads to the result in (4), which can be written in matrix format as shown in (5), where $\mathbf{L}_T$ — termed the per unit length (pul) transverse inductance matrix of the MGTL — is a square real matrix, and $\boldsymbol{\phi}$ and $\mathbf{U}$, in (5)–(6), are column vectors gathering respectively the wire fluxes and wire magnetic voltages.

$$\lim_{\Delta z \to 0} \frac{\phi_k^{\text{stray}}}{\Delta z} = -\frac{\partial}{\partial z}\phi_k(t,z) = \sum_i L_{ki} u_i(t,z) \tag{4}$$

$$\frac{\partial}{\partial z}\boldsymbol{\phi} = -\mathbf{L}_T \mathbf{U}; \quad (\mathbf{L}_T)_{ki} = L_{ki} = \mu_0 g_{ki} \tag{5}$$

$$\begin{aligned} \boldsymbol{\phi} &= [\phi_1(t,z) \ \ldots \ \phi_k(t,z) \ \ldots \ \phi_N(t,z)\,]^T, \\ \mathbf{U} &= [u_1(t,z) \ \ldots \ u_k(t,z) \ \ldots \ u_N(t,z)]^T \end{aligned} \tag{6}$$

Introducing the time-derivative of the magnetic flux (or magnetic flux time rate)

$$\boldsymbol{\varphi} = [\varphi_1(t,z) \ \ldots \ \varphi_k(t,z) \ \ldots \ \varphi_N(t,z)]^T = \frac{\partial}{\partial t}\boldsymbol{\phi} \tag{7}$$

Equation (5) transforms into

$$\frac{\partial}{\partial z}\boldsymbol{\varphi} = -\mathbf{L}_T \frac{\partial}{\partial t}\mathbf{U} \tag{8}$$

At this stage, several remarks are in order. The results in (5) and (8) not only are unaffected by existing system losses, but also are independent of the inhomogeneous character of the dielectric medium. Moreover, the pul transverse inductance matrix $\mathbf{L}_T$ of the MGTL is not to be confused with the familiar pul longitudinal inductance matrix $\mathbf{L}_L$ of electric MTLs. Nonetheless, for ELTLs and MGTLs sharing the same geometry, matrices $\mathbf{L}_T$ and $\mathbf{L}_L$ are intimately correlated (see [14], about the role played by the geometrical factors g). The relationship between matrices $\mathbf{L}_T$ and $\mathbf{L}_L$ is given in (9a), where $\mathbf{1}$ is the identity matrix of rank N. The result in (9a) is equivalent to the one in (9b), where $\mathbf{C}_0$ is the familiar pul transverse capacitance matrix of an ELTL with the same geometry but with the dielectric medium replaced by a vacuum. From the preceding results, the general properties of $\mathbf{L}_T$ can be stated: it is a symmetric positive-define matrix whose entries obey (9c) [20, 21]. Note that the entries of $\mathbf{L}_T$ do not

relate magnetic linkage fluxes with currents (longitudinal currents do not exist in MGTL theory).

$$\mathbf{L}_T\mathbf{L}_L = \mu_0^2\mathbf{1} \tag{9a}$$

$$\mathbf{L}_T = \frac{\mu_0}{\varepsilon_0}\mathbf{C}_0 \tag{9b}$$

$$(\mathbf{L}_T)_{kk} \geq 0,\ (\mathbf{L}_T)_{ki} = (\mathbf{L}_T)_{ik} \leq 0,\ \sum_i (\mathbf{L}_T)_{ki} \geq 0 \tag{9c}$$

2.2. Time-domain Magnetic Voltage Equation

Consider an infinitesimal segment of an MGTL of length Δz (see Figure 3).

Consider a closed rectangular path $\mathbf{s}$ along the periphery of wires k and 0 and through the inhomogeneous dielectric medium where magnetic voltages $u_k(t,z)$ and $u_k(t,z+\Delta z)$ are defined. Since the open rectangular surface S_k bounded by $\mathbf{s}$ is only crossed by displacement currents, the application of $\nabla \times \mathbf{H} = \partial\mathbf{D}/\partial t$ leads to

$$\oint_{\mathbf{s}} \mathbf{H}\cdot d\mathbf{s} = \int_{S_k} \frac{\partial \mathbf{D}}{\partial t}\cdot \mathbf{n}_S dS = -\frac{\partial}{\partial t}\int_{S_k} D_n dS = -\frac{\partial}{\partial t}\psi_k^D \tag{10a}$$

$$u_k(t,z+\Delta z) - u_k(t,z) + (R_{m_k}\phi_k + R_{m_0}\phi_0)\,\Delta z = -\frac{\partial}{\partial t}\psi_k^D \tag{10b}$$

$$D_n = \varepsilon(x,y)\sum_i (\mathbf{E}_i(\varphi_i))\cdot \mathbf{n};\ \text{with } \mathbf{n} = -\mathbf{n}_S \tag{10c}$$

In (10b), the terms $R_{m_k}\phi_k$ and $R_{m_0}\phi_0$ denote the pul longitudinal magnetic voltage drops along wires k and 0, R_{m_k} and R_{m_0} being the pul magnetic reluctances of wires k and 0, respectively. In (10a), the normal component of the displacement vector, D_n, is defined in (10c)

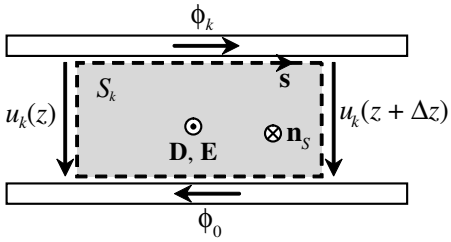

Figure 3. Application of the generalized Ampère law to an infinitesimal segment of an MGTL of length Δz.

as the result of the superposition of transverse electric induction field contributions due to $\varphi_1, \ldots, \varphi_N$, affected by the presence of the dielectric medium (a linear medium). According to $\nabla \cdot \mathbf{B} = 0$, the magnetic flux carried by the reference wire is given by

$$\phi_0(t,z) = \sum_i \phi_i(t,z) \tag{11}$$

As a direct consequence of (10c), the flux of the electric displacement vector across S_k can be written as a linear combination of the wires' magnetic fluxes time-rate

$$\psi_k^D = \Delta z \sum_i C_{ki}\varphi_i(t,z) \tag{12}$$

where the coefficients C_{ki} have physical dimensions of F/m and are termed pul longitudinal capacitances. Also, according to the reciprocity principle: $C_{ki} = C_{ik}$.

Substituting (11)–(12) into (10b), making $\Delta z \to 0$, permits the determination of $\partial u_k/\partial z$ as given by (13). This result can be written compactly in matrix notation as shown in (14)

$$\frac{\partial u_k(t,z)}{\partial z} = -\left(R_{m_k}\phi_k + R_{m_0}\sum_i \phi_i + \frac{\partial}{\partial t}\sum_i C_{ki}\varphi_i\right) \tag{13}$$

$$\frac{\partial}{\partial z}\mathbf{U} = -\left(\mathbf{R}_m \int \boldsymbol{\varphi} dt + \mathbf{C}_L \frac{\partial}{\partial t}\boldsymbol{\varphi}\right) \tag{14}$$

where $\mathbf{C}_L$, the pul longitudinal capacitance matrix, gathers the C_{ki} coefficients mentioned in (12), and where the pul magnetic reluctance matrix $\mathbf{R}_m$ is determined through

$$\mathbf{R}_m = \begin{bmatrix} R_{m_1} & 0 & \ldots & 0 \\ 0 & R_{m_2} & \ldots & 0 \\ \vdots & \vdots & \ddots & \vdots \\ 0 & 0 & \ldots & R_{m_N} \end{bmatrix} + R_{m_0} \begin{bmatrix} 1 & 1 & \ldots & 1 \\ 1 & 1 & \ldots & 1 \\ \vdots & \vdots & \ddots & \vdots \\ 1 & 1 & \ldots & 1 \end{bmatrix} \tag{15}$$

Note that the real symmetric reluctance matrix is not connected with system losses; it is related to internal magnetic energy storage inside the magnetic wires.

The inhomogeneous character of the MGTL is reflected on the $\mathbf{C}_L$ matrix, whose entries depend on the geometry and on $\varepsilon(x,y)$. The longitudinal capacitance matrix is not to be confused with the familiar transverse capacitance matrix $\mathbf{C}_T$ of an ELTL, in fact, no electric charges are at play in MGTL theory.

2.3. Time-domain Ideal Homogeneous MGTL

Time-domain equations derived in Subsections 2.1 and 2.2 are summarized in (16).

$$\begin{cases} \frac{\partial}{\partial z}\boldsymbol{\varphi} = -\mathbf{L}_T \frac{\partial}{\partial t}\mathbf{U} \\ \frac{\partial}{\partial z}\mathbf{U} = -\left(\mathbf{R}_m \int \boldsymbol{\varphi} dt + \mathbf{C}_L \frac{\partial}{\partial t}\boldsymbol{\varphi}\right) \end{cases} \tag{16}$$

For ideal MGTLs ($\mu_m = \infty$), $\mathbf{R}_m = 0$ is obtained. Hence, from (16),

$$\begin{cases} \frac{\partial}{\partial z}\boldsymbol{\varphi} = -\mathbf{L}_T \frac{\partial}{\partial t}\mathbf{U} \\ \frac{\partial}{\partial z}\mathbf{U} = -\mathbf{C}_L \frac{\partial}{\partial t}\boldsymbol{\varphi} \end{cases} \tag{17}$$

Combining the two equations in (17) leads to the wave equation

$$\frac{\partial^2}{\partial z^2}\begin{Bmatrix} \boldsymbol{\varphi}(z,t) \\ \mathbf{U}(z,t) \end{Bmatrix} = \begin{Bmatrix} \mathbf{L}_T\mathbf{C}_L \\ \mathbf{C}_L\mathbf{L}_T \end{Bmatrix} \frac{\partial^2}{\partial t^2}\begin{Bmatrix} \boldsymbol{\varphi}(z,t) \\ \mathbf{U}(z,t) \end{Bmatrix} \tag{18a}$$

Since the matrix products $\mathbf{L}_T\mathbf{C}_L$ and $\mathbf{C}_L\mathbf{L}_T$ are the transposed of each other, both products must share the same set of eigenvalues; these eigenvalues define the squared modal propagation velocities [21]. However, for ideal homogeneous transmission lines, the squared modal propagation velocities degenerate into $v_w^2 = 1/(\mu_0\varepsilon)$. Therefore, the result in (18a) should translate into

$$\frac{\partial^2}{\partial z^2}\begin{Bmatrix} \boldsymbol{\varphi}(z,t) \\ \mathbf{U}(z,t) \end{Bmatrix} = \mu_0\varepsilon \frac{\partial^2}{\partial t^2}\begin{Bmatrix} \boldsymbol{\varphi}(z,t) \\ \mathbf{U}(z,t) \end{Bmatrix} \tag{18b}$$

from where follows the conclusion that the products $\mathbf{L}_T\mathbf{C}_L$ and $\mathbf{C}_L\mathbf{L}_T$ are identical diagonal matrices — see (19a). In addition, taking (9b) into account, we find

$$\mathbf{L}_T\mathbf{C}_L = \mathbf{C}_L\mathbf{L}_T = \mu_0\varepsilon\mathbf{1} \tag{19a}$$

$$\mathbf{C}_0\mathbf{C}_L = \mathbf{C}_L\mathbf{C}_0 = \varepsilon\varepsilon_0\mathbf{1} \rightarrow \mathbf{C}_L = \varepsilon\left(\varepsilon_0\mathbf{C}_0^{-1}\right) \tag{19b}$$

2.4. Physical Interpretation of the L_T and C_L Matrices

A simple example describing the evaluation of the entries of matrices $\mathbf{L}_T$ and $\mathbf{C}_L$, based on field calculations, is offered in Appendix A.

In the familiar case of an ELTL, the pul longitudinal inductance matrix $\mathbf{L}_L$ relates magnetic fluxes linked with system subcircuits (circuits k-0), with system longitudinal currents. In the case of an MGTL longitudinal currents are absent; the interpretation for the pul transverse inductance matrix $\mathbf{L}_T$ can be found in terms of magnetic energy storage in the volume of the dielectric medium — due to the presence of stray magnetic field lines between magnetic wires, which

give rise to magnetic voltages. The pul magnetic energy stored is given by the quadratic form

$$W_m = \int_V \frac{1}{2}\mathbf{B}\cdot\mathbf{H}dV = \frac{1}{2}\mathbf{U}^T\mathbf{L}_T\mathbf{U}$$

In the familiar case of an ELTL, the pul transverse capacitance matrix $\mathbf{C}_T$ relates conductor electric charges with system electric voltages. In the case of an MGTL electric charges are absent; the interpretation for the pul longitudinal capacitance matrix $\mathbf{C}_L$ can be found in terms of electric energy storage in the volume of the dielectric medium — due to the presence of electric induction field lines encircling the magnetic wires, created by time-varying magnetic fluxes flowing longitudinally along the wires. The pul electric energy stored is given by the quadratic form

$$W_e = \int_V \frac{1}{2}\mathbf{D}\cdot\mathbf{E}dV = \frac{1}{2}\boldsymbol{\varphi}^T\mathbf{C}_L\boldsymbol{\varphi}$$

2.5. Frequency-domain MGTL Equations

The time-domain equations in (16) are now applied to harmonic regimes ($e^{j\omega t}$). The analysis in the frequency domain allows for the inclusion of system losses which, otherwise, cannot be easily incorporated in time-domain equations [22].

Magnetic wires are immersed in an inhomogeneous nonmagnetic linear lossy dielectric medium, characterized by a complex permittivity $\bar{\varepsilon} = \bar{\varepsilon}(x, y)$ and $\mu = \mu_0$. Consequently, the pul longitudinal capacitance matrix introduced in (14) is replaced by a pul complex longitudinal capacitance matrix, $\bar{\mathbf{C}}_L$, whose imaginary part accounts for dielectric losses.

Lossy magnetic wires are characterized by a complex permeability $\bar{\mu}_m$ and complex permittivity $\bar{\varepsilon}_m$. Consequently, the pul magnetic reluctance matrix introduced in (15) is replaced by a pul complex magnetic reluctance matrix $\bar{\mathbf{R}}_m$, whose computation involves skin effect theory. Note that magnetic wire losses are accounted through the imaginary part of $\bar{\mathbf{R}}_m$, which is always positive [14, 16].

Therefore, the results in (16), can be written in phasorial form as

$$\begin{cases} \frac{d}{dz}\bar{\boldsymbol{\varphi}} = -\bar{\mathbf{Z}}_T\bar{\mathbf{U}} \\ \frac{d}{dz}\bar{\mathbf{U}} = -\bar{\mathbf{Y}}_L\bar{\boldsymbol{\varphi}} \end{cases} ; \quad \begin{cases} \bar{\mathbf{Z}}_T = j\omega\mathbf{L}_T \\ \bar{\mathbf{Y}}_L = \bar{\mathbf{G}}_L + j\omega\bar{\mathbf{C}}_L \end{cases} \tag{20}$$

where $\bar{\mathbf{G}}_L$, (units: S/m), is the pul complex longitudinal magnetic conductance matrix:

$$\bar{\mathbf{G}}_L = \frac{\bar{\mathbf{R}}_m}{j\omega} \tag{21}$$

In (20), $\bar{\mathbf{Z}}_T$ is the pul transverse impedance matrix of the MGTL (units: Ω/m), and $\bar{\mathbf{Y}}_L$ is the pul longitudinal admittance matrix of the MGTL (units: S/m).

The well-known [19–21], frequency-domain multiconductor ELTL equations are reminded bellow. For comparison purposes, they should be confronted with (20).

$$\begin{cases} \frac{d}{dz}\bar{\mathbf{I}} = -\bar{\mathbf{Y}}_T\bar{\mathbf{V}} \\ \frac{d}{dz}\bar{\mathbf{V}} = -\bar{\mathbf{Z}}_L\bar{\mathbf{I}} \end{cases} ; \quad \begin{cases} \bar{\mathbf{Y}}_T = \mathbf{G}_T + j\omega\bar{\mathbf{C}}_T \\ \bar{\mathbf{Z}}_L = \bar{\mathbf{R}}_L + j\omega\mathbf{L}_L \end{cases} \tag{22}$$

2.6. Analogy between Electric and Magnetic MTLs

Table 1 briefly summarizes the correspondence between field vectors, variables, and matrices, concerning electric and magnetic MTLs.

Also, for comparison purposes, the structural form of equivalent T circuits corresponding to magnetic and electric MTLs of elemental length Δz, (case $N = 1$), is offered in Figure 4.

The circuit in Figure 4(b) behaves as a low-pass filter, whereas the circuit in Figure 4(a) behaves, essentially, as a high-pass filter. This result suggests that MGTLs are expected to perform better at high frequencies than at low frequencies. Nonetheless, the reader should be aware that wire magnetic reluctance $\bar{R}_m(\omega)$, involved in the determination of $\bar{G}_L$, may have quite complicated frequency behavior [16], something not happening to electric conductor internal impedance $\bar{R}_L(\omega)$.

Table 1. Analogy between electric and magnetic MTLs.

MTL	Fields				Variables		Matrices	
Electric	$\mathbf{J}$	$\mathbf{E}$	$\mathbf{H}$	$\mathbf{B}$	$\bar{\mathbf{V}}$	$\bar{\mathbf{I}}$	$\bar{\mathbf{Z}}_L$	$\bar{\mathbf{Y}}_\mathbf{T}$
Magnetic	$\frac{\partial\mathbf{B}}{\partial t}$	$\mathbf{H}$	$-\mathbf{E}$	$-\frac{\partial\mathbf{D}}{\partial t}$	$\bar{\mathbf{U}}$	$\bar{\varphi}$	$\bar{\mathbf{Y}}_L$	$\bar{\mathbf{Z}}_T$

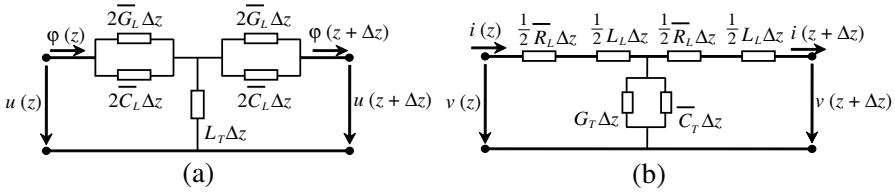

Figure 4. Equivalent circuits. (a) MGTL. (b) ELTL.

3. SOLUTION OF MGTL PROPAGATION EQUATIONS

The solution of the coupled equations in (20) can be obtained by employing a modal analysis technique, similar to the one utilized in the study of electric MTLs. Such a technique is well-known [19–21] and, therefore, only a brief summary is presented here. In what follows, and in order to alleviate the notation, we will drop the over-bar symbols denoting complex quantities.

Let $\mathbf{T}$ and $\mathbf{W}$ represent the transformation matrices that transform natural quantities into modal quantities, the latter being identified by hat symbols

$$\boldsymbol{\varphi} = \mathbf{T}\hat{\boldsymbol{\varphi}}, \quad \mathbf{U} = \mathbf{W}\hat{\mathbf{U}} \tag{23}$$

The complex modal propagation constants $\gamma_1 \ldots \gamma_k \ldots \gamma_N$ of the N travelling modes are determined upon the diagonalization of the product matrices $\mathbf{Z}_T\mathbf{Y}_L$, or $\mathbf{Y}_L\mathbf{Z}_T$, i.e.,

$$\left\{ \begin{array}{c} \mathbf{T}^{-1}(\mathbf{Z}_T\mathbf{Y}_L)\mathbf{T} \\ \mathbf{W}^{-1}(\mathbf{Y}_L\mathbf{Z}_T)\mathbf{W} \end{array} \right\} = \boldsymbol{\gamma}^2 = \mathrm{diag}\left\{\gamma_1^2 \ldots \gamma_k^2 \ldots \gamma_N^2\right\} \tag{24a}$$

The columns of $\mathbf{T} = \{\mathbf{t}_1 \ldots \mathbf{t}_k \ldots \mathbf{t}_N\}$ are the eigenvectors of $\mathbf{Z}_T\mathbf{Y}_L$, and the columns of $\mathbf{W} = \{\mathbf{w}_1 \ldots \mathbf{w}_k \ldots \mathbf{w}_N\}$ are the eigenvectors of $\mathbf{Y}_L\mathbf{Z}_T$, that is

$$\left\{ \begin{array}{c} \mathbf{Z}_T\mathbf{Y}_L \\ \mathbf{Y}_L\mathbf{Z}_T \end{array} \right\} \left\{ \begin{array}{c} \mathbf{t}_k \\ \mathbf{w}_k \end{array} \right\} = \gamma_k^2 \left\{ \begin{array}{c} \mathbf{t}_k \\ \mathbf{w}_k \end{array} \right\} \tag{24b}$$

Since $\mathbf{Z}_T\mathbf{Y}_L$ and $\mathbf{Y}_L\mathbf{Z}_T$ are the transposed of each other, one can always choose $\mathbf{W}^{-1} = \mathbf{T}^T$ [21]. Per unit length transverse modal impedances and longitudinal modal admittances are evaluated through

$$\hat{\mathbf{Z}}_T = \mathbf{T}^{-1}\mathbf{Z}_T\mathbf{W}, \quad \hat{\mathbf{Y}}_L = \mathbf{W}^{-1}\mathbf{Y}_L\mathbf{T} \tag{25}$$

The diagonal modal characteristic wave admittance matrix $\hat{\mathbf{Y}}_w = \mathrm{diag}\{\hat{Y}_{w_1} \ldots \hat{Y}_{w_k} \ldots \hat{Y}_{w_N}\}$ is obtained through [19–21],

$$\hat{\mathbf{Y}}_w = \left(\hat{\mathbf{Y}}_L\hat{\mathbf{Z}}_T^{-1}\right)^{1/2} = \left(\mathbf{T}^T\mathbf{Z}_T^{-1}\mathbf{T}\right)\boldsymbol{\gamma} = \left(\mathbf{T}^T\mathbf{Y}_L\mathbf{T}\right)\boldsymbol{\gamma}^{-1} \tag{26}$$

By making use of the above results, we can write the phasors $\boldsymbol{\varphi}(z)$ and $\mathbf{U}(z)$ in the form of a superposition of modes

$$\left\{ \begin{array}{l} \boldsymbol{\varphi}(z) = \sum\limits_{k=1}^{N} \mathbf{t}_k \left(e^{-\gamma_k z}\hat{\varphi}_{k(i)} + e^{+\gamma_k z}\hat{\varphi}_{k(r)}\right) \\ \mathbf{U}(z) = \sum\limits_{k=1}^{N} \mathbf{w}_k \hat{Y}_{w_k} \left(e^{-\gamma_k z}\hat{\varphi}_{k(i)} - e^{+\gamma_k z}\hat{\varphi}_{k(r)}\right) \end{array} \right. \tag{27}$$

where the modal magnetic flux rate phasors $\hat{\varphi}_{k(i)}$ and $\hat{\varphi}_{k(r)}$, of the incident and reflected waves at $z = 0$, are determined from enforced boundary conditions.

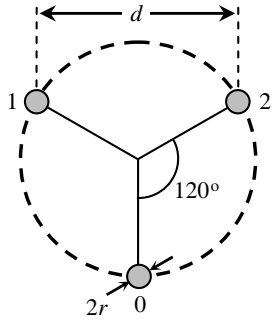

Figure 5. Cross section of a 3-wire system with three-fold symmetry.

4. APPLICATION EXAMPLE

A simple MGTL configuration consisting of three equidistant circular cylindrical magnetic wires (Figure 5) is used to illustrate the application of the theory developed in the preceding sections. In a cross sectional view, the wires occupy the vertices of an equilateral triangle. The distance between wires is d, and the radius of each wire is r.

The medium where the wires are immersed is the air (ε_0, μ_0). All the magnetic wires are characterized by $\bar{\mu}_m = \mu'(\omega) - j\mu''(\omega)$ and $j\omega\bar{\varepsilon}_m = \sigma_m + j\omega\varepsilon_r\varepsilon_0$. Given the geometry of the system, the familiar electrostatic transverse capacitance matrix $\mathbf{C}_0$ and its inverse can be written as in (28a), where $c_p = \varepsilon_0 g$ denotes the pul partial capacitance between any wire pair, where g is a geometrical factor [23, 24], given by (28b)

$$\mathbf{C}_0 = c_p \begin{bmatrix} 2 & -1 \\ -1 & 2 \end{bmatrix}, \quad \mathbf{C}_0^{-1} = \frac{1}{3c_p} \begin{bmatrix} 2 & 1 \\ 1 & 2 \end{bmatrix} \tag{28a}$$

$$g \approx \pi/\text{arccosh}(\upsilon), \quad \upsilon = d/(2r) \tag{28b}$$

Note: The result in (28b) is a good approximation (error smaller than 2%) for $\upsilon > 2.5$ [24]. Results concerning the computation of c_p (for any value of υ) are reported in [24], where an electrostatic harmonic expansion method was employed to accurately account for proximity effects.

From (9b) and (19b), the pul transverse inductance matrix $\mathbf{L}_T$ and the pul longitudinal capacitance matrix $\mathbf{C}_L$ are evaluated through

$$\mathbf{L}_T = \mu_0 g \begin{bmatrix} 2 & -1 \\ -1 & 2 \end{bmatrix}, \quad \mathbf{C}_L = \frac{\varepsilon_0}{3g} \begin{bmatrix} 2 & 1 \\ 1 & 2 \end{bmatrix} \tag{29}$$

From (15), the pul magnetic reluctance matrix of the system is given by (30a), where $\bar{R}_m(\omega)$ is the frequency-dependent pul complex reluctance of each magnetic wire [14, 16], which is given by (30b), where F_{prox} is a correction factor related to proximity effects [25], given by (30c), and $\bar{\kappa}$ is a dimensionless frequency-dependent parameter [14], given by (30d).

$$\bar{\mathbf{R}}_m = \bar{R}_m(\omega) \begin{bmatrix} 2 & 1 \\ 1 & 2 \end{bmatrix} \tag{30a}$$

$$\bar{R}_m(\omega) \approx \frac{1}{\pi r^2 \mu_{DC}} \bar{\kappa} \frac{J_0(\bar{\kappa})}{2J_1(\bar{\kappa})} F_{\text{prox}} \tag{30b}$$

$$F_{\text{prox}} = \upsilon / \sqrt{\upsilon^2 - 1} \tag{30c}$$

$$\bar{\kappa}(\omega) = r\omega \sqrt{\bar{\mu}_m(\omega) \bar{\varepsilon}_m(\omega)} \tag{30d}$$

For the geometry under analysis, the 2×2 product matrix $\bar{\mathbf{Z}}_T \bar{\mathbf{Y}}_L$ transforms into a diagonal scalar matrix:

$$\bar{\mathbf{Z}}_T \bar{\mathbf{Y}}_L = \mathbf{L}_T \bar{\mathbf{R}}_m - \omega^2 \mathbf{L}_T \bar{\mathbf{C}}_L = \left(3\mu_0 g \bar{R}_m - \omega^2 \mu_0 \varepsilon_0\right) \mathbf{1} \tag{31}$$

Since $\bar{\mathbf{Z}}_T \bar{\mathbf{Y}}_L$ is already in diagonal form, any nonsingular modal transformation matrix can be utilized. Here, a modal transformation leading to a decomposition into familiar even and odd modes is chosen, that is

$$\mathbf{T} = \mathbf{T}^{-1} = \mathbf{T}^T = \frac{1}{\sqrt{2}} \begin{bmatrix} 1 & 1 \\ 1 & -1 \end{bmatrix} \tag{32}$$

Mode 1, with $\mathbf{t}_1 \propto [\ 1 \quad 1\ ]^T$, is the even mode, whereas mode 2, with $\mathbf{t}_2 \propto [1\ -1]^T$, is the odd mode. Figure 6 illustrates electric and magnetic field lines observed at a transverse plane of the line, for both traveling modes.

The two modes share the same propagation constant:

$$\bar{\gamma} = \alpha + \frac{j\omega}{v} = \frac{j\omega}{c} \sqrt{1 - \frac{3g\bar{R}_m(\omega)}{\omega^2 \varepsilon_0}} \tag{33a}$$

$$\alpha \approx \sqrt{\frac{\mu_0}{\varepsilon_0}} \frac{3g}{2\omega} \text{Im}\left(\bar{R}_m(\omega)\right), \quad \frac{v}{c} \approx 1 + \frac{3g}{2\varepsilon_0 \omega^2} \text{Re}\left(\bar{R}_m(\omega)\right) \tag{33b}$$

In (33), α and v denote the pul attenuation constant and the phase velocity of both modes, whereas c denotes the free-space velocity. Physical insight on how α and v depend on the frequency is provided by the results in (33b), which are a simplification of (33a), valid when

$$\omega^2 \gg 3g|\bar{R}_m|/\varepsilon_0 \tag{34}$$

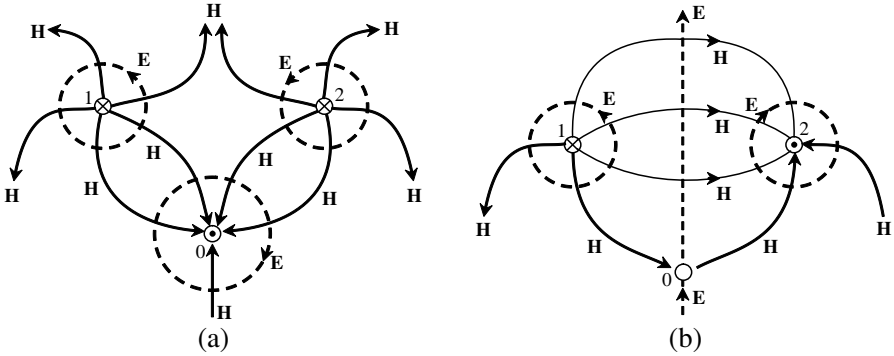

Figure 6. Field lines of **E** and **H**. (a) Even mode. (b) Odd mode.

The different modal characteristic wave admittances are obtained from (26), yielding $\hat{Y}_{w_1} = \bar{\gamma}/(j\omega\mu_0 g)$ and $\hat{Y}_{w_2} = \hat{Y}_{w_1}/3$. Numerical simulation results concerning the frequency dependence of the modal propagation constant are presented here. The following data have been considered:

$$\text{Geometry} \begin{cases} r = 0.5\,\text{mm} \\ d = 5\,\text{mm} \end{cases} ; \quad \upsilon = 5 \tag{35}$$

Magnetic wires, made of ferrite, are assigned the following parameters [16]:

$$\bar{\mu}_m \approx \mu_0 + \frac{\mu_{DC}}{1+(f/f_\times)^2} - j\frac{\mu_{DC}}{1+(f/f_\times)^2}\left(\frac{f}{f_\times}\right) \tag{36a}$$

$$\mu_{DC} = 10^4\mu_0, \quad f_\times = 0.2\,\text{MHz} \tag{36b}$$

$$\varepsilon_r = 10, \quad \sigma_m = 5\times 10^{-3}\,\text{S/m} \tag{36c}$$

Figure 7 shows the pul magnetic reluctance of the wires, obtained from (30), in the range 0.1 to 10 GHz (our analysis window). The parameters in (36c) are assumed to remain practically invariant in the frequency range considered. Frequencies above 10 GHz were not explored to ensure that distance d remains a small fraction of the wavelength ($d < \lambda/10$) in order to keep using the quasi TEM-approach.

The attenuation constant $\alpha(\omega)$ and the normalized phase velocity $v(\omega)/c$, shared by both modes, were evaluated and plotted against frequency in the range 0.1 GHz to 10 GHz — see Figure 8. The dashed lines correspond to the approximation given by (33b). For the data being considered, the attenuation constant reveals a practically constant minimum value of about 0.03 dB/m at frequencies around 1 GHz. Contrary to the attenuation constant, the normalized phase

velocity (which is higher than unity — superluminal velocity) is seen to monotonically decrease with the frequency, converging to 1.

The fact that $v(\omega)$ exceeds c should not be a concern. As it is well-known, the phase velocity does not have intrinsic physical meaning, contrarily to the group velocity or velocity of energy travel (equivalent concepts in the case of normal dispersion, $dv/d\omega < 0$) [25].

For comparison purposes, the propagation constant of a three-wire

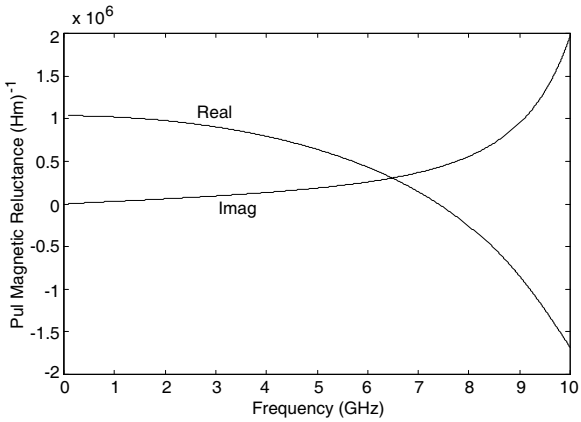

Figure 7. Per unit length magnetic reluctance against frequency.

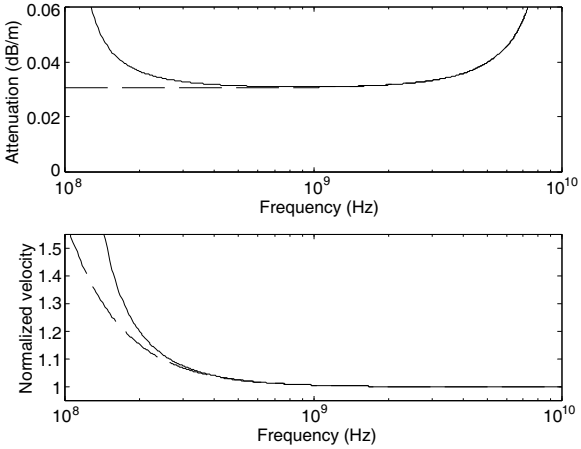

Figure 8. MGTL propagation constant. The upper subplot refers to the modal attenuation constant against frequency, whereas the bottom subplot refers to the normalized phase velocity against frequency. The dashed lines correspond to the approximation in (33b).

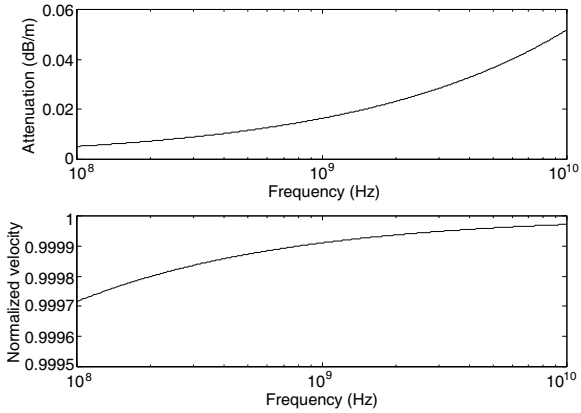

Figure 9. ELTL propagation constant. The upper subplot refers to the modal attenuation constant against frequency, whereas the bottom subplot refers to the normalized phase velocity against frequency.

ELTL with the same geometry (Figure 5) was also evaluated, taking skin effect phenomena into account [19]. Instead of magnetic wires, electric conductors are considered now. Simulation results, depicted in Figure 9, were obtained considering that conductors are made of aluminium ($\sigma = 3.5 \times 10^7$ S/m).

The discussion of the advantages or disadvantages of MGTLs versus electric transmission lines makes little sense unless concrete design goals are set. However, for the frequency window that has been considered, the comparison between the propagation constants of the magnetic and electric MTL shown in Figures 8 and 9 provides some clues. If the design goal is to ensure a zero, or almost zero, attenuation dispersion system ($d\alpha/d\omega$) the MGTL system is the preferred candidate. Likewise, if a superluminal phase velocity is the design goal, the MGTL system is, again, the preferred candidate. Conversely, if small velocity dispersion ($dv/d\omega$), or subluminal phase velocity, are the design goals, the ELTL system is the preferred candidate.

5. CONCLUSION

A novel theoretical development on magnetic transmission line analysis aimed at the generalization of former research work on two-wire homogeneous MGTLs to multiwire inhomogeneous systems was presented. Contrary to electric MTLs, it was shown that the analysis of magnetic MTLs involves the consideration of pul transverse inductance

and impedance matrices, as well as pul longitudinal capacitance and admittance matrices. Modal propagation constants and modal characteristic wave admittances concerning magnetic MTLs were derived by making use of matrix modal analysis techniques.

An example of a multiwire magnetic transmission line, consisting of three identical equidistant cylindrical wires, was considered in order to illustrate the application of the developed theory, the frequency-dependence of wires' complex permeability being taken into account. The geometry under analysis was described by two degenerate propagation modes (even and odd modes) whose wave propagation parameters were evaluated as a function of the frequency (from 0.1 to 10 GHz). These wave parameters were compared with the corresponding ones concerning a multiconductor electric transmission line with the same geometry. Results showed that the MGTL has a superluminal phase velocity and zero, or almost zero, attenuation dispersion in a wide frequency band.

APPENDIX A. EXAMPLE OF THE CALCULATION OF $\mathbf{C}_L$ AND $\mathbf{L}_T$ MATRICES

Similarly to ELTLs, the analytical determination of the pul capacitances and inductances of MGTLs is only possible for very simple geometries. For general geometries, numerical or hybrid computational methods are usually required. A simple example concerning the calculation of the $\mathbf{C}_L$ and $\mathbf{L}_T$ matrices of an inhomogeneous ideal MGTL is offered here — see the MTL geometry depicted in Figure A1.

The cylindrical wires 1 and 2, positioned at ($x = x_1$, $y = 0$, and $x = x_2$, $y = 0$, respectively) carry z-oriented magnetic fluxes ϕ_1 and ϕ_2, the corresponding magnetic voltages (k-0) are u_1 and u_2. The inhomogeneous dielectric medium is characterized by $\varepsilon = \varepsilon_a$ for $y < 0$, and $\varepsilon = \varepsilon_b$ for $y > 0$. For simplification purposes the thin wires assumption is considered (negligibly small radii).

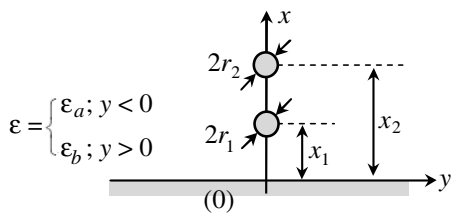

Figure A1. Two cylindrical magnetic wires parallel to a magnetic plane.

- Calculation of $\mathbf{C}_L$

From $\nabla \times \mathbf{E} = -\partial \mathbf{B}/\partial t$, $\mathbf{D} = \varepsilon \mathbf{E}$, and from the continuity condition of the normal component of the $\mathbf{D}$ vector across the interface $y = 0$, the $\mathbf{D}$ vector can easily be determined in the $y = 0$ plane as a function of $\varphi_k = \partial \phi_k/\partial t$, with $k = 1, 2$:

$$\mathbf{D} = D(x)\vec{e}_y; \quad D(x) = \frac{\varepsilon_{ef}}{\pi} \sum_{k=1}^{2} \left(\frac{x_k}{x_k^2 - x^2} \varphi_k \right) \tag{A1}$$

where the effective permittivity is given by

$$\varepsilon_{ef} = 2\frac{\varepsilon_a \varepsilon_b}{\varepsilon_a + \varepsilon_b} \tag{A2}$$

According to (12), considering a magnetic MTL of unitary length, we have

$$\begin{cases} \psi_1^D = C_{11}\varphi_1 + C_{12}\varphi_2 \\ \psi_2^D = C_{21}\varphi_1 + C_{22}\varphi_2 \end{cases} \tag{A3}$$

where the electric displacement fluxes ψ_j^D are determined by integrating $D(x)$ along x:

$$\psi_j^D = \frac{\varepsilon_{ef}}{2\pi} \sum_{k=1}^{2} \left(\int_0^{x_j - r_j} \frac{2x_k}{x_k^2 - x^2} dx \right) \varphi_k \tag{A4}$$

From (A3) and (A4), we obtain

$$\mathbf{C}_L = \frac{\varepsilon_{ef}}{2\pi} \begin{bmatrix} \ln\left(\frac{2x_1}{r_1}\right) & \ln\left(\frac{x_2+x_1}{|x_2-x_1|}\right) \\ \ln\left(\frac{x_2+x_1}{|x_2-x_1|}\right) & \ln\left(\frac{2x_2}{r_2}\right) \end{bmatrix} \tag{A5}$$

- Calculation of $\mathbf{L}_T$

If the inhomogeneous dielectric medium is replaced by a vacuum, we see from (19a) that

$$\mathbf{L}_T = \mu_0 \varepsilon_0 \left(\mathbf{C}_L\right)_{\varepsilon=\varepsilon_0}^{-1} \tag{A6}$$

Then, from (A5), we get

$$\mathbf{L}_T = \frac{2\pi\mu_0}{\Delta} \begin{bmatrix} \ln\left(\frac{2x_2}{r_2}\right) & -\ln\left(\frac{x_2+x_1}{|x_2-x_1|}\right) \\ -\ln\left(\frac{x_2+x_1}{|x_2-x_1|}\right) & \ln\left(\frac{2x_1}{r_1}\right) \end{bmatrix} \tag{A7}$$

where $\Delta = \ln(\frac{2x_2}{r_2}) \ln(\frac{2x_1}{r_1}) - \ln^2(\frac{x_2+x_1}{|x_2-x_1|})$.

REFERENCES

1. Pipes, L. A., "Matrix theory of multiconductor transmission lines," *Phil. Mag. S. 7*, Vol. 24, 97–113, 1937.
2. Rice, S. O., "Steady state solutions of transmission line equations," *Bell Syst. Tech. J.*, Vol. 20, 131–178, 1941.
3. Wedepohl, L. M., "Application of matrix methods to the solution of travelling-wave phenomena in polyphase systems," *Proc. Inst. Elect. Eng.*, Vol. 10, 2200–2212, 1963.
4. Hedman, D. E., "Propagation on overhead transmission lines, I — Theory of modal analysis," *IEEE Trans. Power App. Syst.*, Vol. 84, 1877–1884, 1965.
5. Dommel, H. W. and W. S. Meyer, "Computation of electromagnetic transients," *Proceedings of the IEEE*, Vol. 62, 983–993, 1974.
6. Gary, C., "Approche complete de la propagation multifilaire en haute frequence par utilization des matrices complexes," *EDF Bulletin de la Direction des Études et Recherches*, No. 3–4, 5–20, 1976.
7. Brandão Faria, J. A. and J. B. da Silva, "Wave propagation in polyphase transmission lines: A general theory to include cases where ordinary modal theory fails," *IEEE Trans. Power Del.*, Vol. 1, 743–764, 1987.
8. Djordjevic, A. R., T. K. Sarkar, and E. F. Harrington, "Time-domain response of multiconductor transmission lines," *Proceedings of the IEEE*, Vol. 75, 643–764, 1987.
9. Khan, O. D., A. Z. Elsherbeni, C. E. Smith, and D. Kajfez, "Characteristics of cylindrical multiconductor transmission lines above a perfectly conducting ground plane," *Progress In Electromagnetics Research*, Vol. 15, 191–220, 1997.
10. Trakadas, P. T. and C. N. Capsalis, "Validation of a modified FDTD method on non-uniform transmission lines," *Progress In Electromagnetics Research*, Vol. 31, 311–329, 2001.
11. Brandão Faria, J. A., "A new generalized modal analysis theory for nonuniform multiconductor transmission lines," *IEEE Trans. Power Syst.*, Vol. 18, 926–933, 2004.
12. Khalaj-Amirhosseini, M., "Analysis of coupled or single nonuniform transmission lines using Taylor's series expansion," *Progress In Electromagnetics Research*, Vol. 60, 107–117, 2006.
13. Dědková, J. and L. Brančík, "Laplace transform and FDTD approach applied to MTL simulation," *PIERS Online*, Vol. 4, No. 1, 16–20, 2008.

14. Brandão Faria, J. A. and M. P. Pires, "Theory of magnetic transmission lines," *IEEE Trans. Microw. Theory Tech.*, Vol. 60, 2941–2949, 2012.
15. Brandão Faria, J. A., "A physical model of the ideal transformer based on magnetic transmission line theory," *Journal of Electromagnetic Waves and Applications*, Vol. 27, No. 3, 2013.
16. Brandao Faria, J. A. M., "Complex reluctance of inhomogeneous Euler-Cauchy tubular ferrites taking into account frequency-dependent complex permeability," *Progress In Electromagnetics Research M*, Vol. 25, 71–85, 2012.
17. Kerns, Q. A., "Transient-suppressing magnetic transmission line," Patent US 3376523, Apr. 1968.
18. Brandão Faria, J. A., "Dispositivo formado por uma linha magnética de transmissão para uso em circuitos integrados para aplicações na tecnologia terahertz [Magnetic transmission line device for terahertz integrated circuits]," Patent PT 106056, Dec. 2011.
19. Brandão Faria, J. A., *Electromagnetic Foundations of Electrical Engineering*, Wiley, Chichester, 2008.
20. Paul, C. R., *Analysis of Multiconductor Transmission Lines*, Wiley, New York, 1994.
21. Brandão Faria, J. A., *Multiconductor Transmission-line Structures: Modal Analysis Techniques*, Wiley, New York, 1993.
22. Brandão Faria, J. A., "On the time-domain transmission-line equations," *Microw. Opt. Tech. Letters*, Vol. 22, 194–197, 1999.
23. Papaleonidopoulos, I., C. Karagiannopoulos, C. Anagnostopoulos, and N. Theodorou, "A theoretical justification of the two-conductor HF transmission-line model for indoor single-phase low voltage triplex cables," *Proc. 7th Int. Symp. Power-line Communications Appl.*, 114–119, Kyoto, Japan, Mar. 2003.
24. Brandão Faria, J. A. and M. G. Neves, "Accurate evaluation of indoor triplex cable capacitances taking conductor proximity effects into account," *IEEE Trans. Power Del.*, Vol. 21, 1238–1244, 2006.
25. Ramo, S., J. Whinnery, and T. Van Duzer, *Fields and Waves in Communications Electronics*, 2nd edition, Wiley, Singapore, 1984.